Journal of Power Sources 258 (2014) 39–45

Contents lists available at ScienceDirect

Journal of Power Sources

journal homepage: www.elsevier.com/locate/jpowsour

Electrospun silicon/carbon/titanium oxide composite nanofibers for lithium ion batteries

Qingliu Wu [a,1], Toan Tran [b,1], Wenquan Lu [a], Ji Wu [b,*]

[a] Electrochemical Energy Storage, Chemical Sciences and Engineering Division, 9700 South Cass Avenue, Building 205, Argonne, IL 60439-4837, USA
[b] Department of Chemistry, Georgia Southern University, Statesboro, GA 30460, USA

HIGHLIGHTS

- We fabricated silicon/graphite/TiO_2 composite nanofibers (NFs) via an electrospinning method.
- Stable TiO_2 shell is beneficial for enhancing the cycling performance of these electrodes.
- These NFs showed superior electrochemical performance as lithium ion battery anode.
- 94% of initial specific capacity (720 mAh g^{-1}) can be maintained after 55 cycles.

GRAPHICAL ABSTRACT

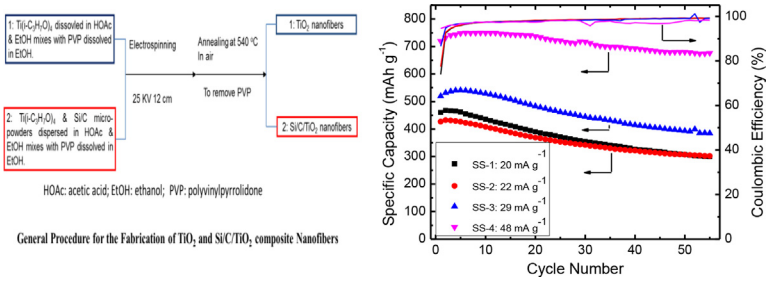

ARTICLE INFO

Article history:
Received 21 December 2013
Received in revised form
1 February 2014
Accepted 11 February 2014
Available online 19 February 2014

Keywords:
Titanium oxide
Silicon
Graphite
Composite nanofiber
Lithium ion battery

ABSTRACT

$Si/C/TiO_2$ composite nanofibers have been prepared via a facile electrospinning method combined with a sol–gel chemistry, whose electrochemical performance as anode materials in lithium-ion battery was evaluated. As-prepared nanofibers (NFs) were characterized using scanning electron microscopy, energy dispersive spectroscopy, powder X-ray diffraction and thermogravimetric analyzer to identify their morphology, phase, crystallinity and compositions. Rutile phase TiO_2 nanofibers demonstrated a relatively low gravimetric specific capacity of ~83 mAh g^{-1} when discharged at 0.1C. In contrast, composite nanofibers possess a much higher gravimetric specific capacity. When the Si to C mass ratio is of 0.217, a specific capacity as high as 720 mAh g^{-1} can be attained, 94% of which can be maintained after 55 cycles. The enhanced cycling stability of micron silicon materials is attributed to the space confinement provided by the structurally stable TiO_2. These findings can provide a beneficial guidance for future lithium ion battery electrode development.

Published by Elsevier B.V.

1. Introduction

The utilization of green energy such as solar and wind power is believed to be one of the most promising approaches to support a more sustainable economic growth [1–4]. Lithium ion batteries (LIBs) have been widely viewed as one of the most promising energy storage technologies for renewable and intermittent energy sources [2,5]. However, several aspects including relatively high cost, low capacity and poor performance limit their broader applications [6,7]. Silicon is a promising candidate for lithium ion battery anode because of its high theoretical capacity (4200 mAh g^{-1}) and low operation voltage [8–10]. But the structure of Si is not stable during the lithiation/delithiation process, mainly due to the nearly 300% lattice volume variation and

* Corresponding author. Tel.: +1 9124780850; fax: +1 9124780699.
E-mail addresses: wuq@anl.gov (Q. Wu), tt01505@georgiasouthern.edu (T. Tran), wenquan.lu@anl.gov (W. Lu), jiwu666@gmail.com, jwu@georgiasouthern.edu (J. Wu).
[1] Both authors contribute equally to this paper.

http://dx.doi.org/10.1016/j.jpowsour.2014.02.047
0378-7753/Published by Elsevier B.V.

unstable solid electrolyte interphase (SEI) films, leading to pulverization, low cycling efficiency, and permanent capacity losses [10–12]. Recently, it has been found that nanostructured silicon as the anode material for LIBs possesses a much improved stability and gravimetric capacity [10,11,13]. It has been demonstrated that micro-sized Si–C composites composed of nanoscale primary building blocks are attractive anodes for lithium ion batteries [14,15]. To obtain high capacity (1200 mAh g^{-1}) and stable cycling performance (600 cycles), the size of Si building blocks should be smaller than 15 nm, and carbon coating can significantly improve the first cycle Coulombic efficiency and the rate capability [14,15]. However, the reduced volumetric energy density and increased fabrication cost could seriously hinder their commercial applications [11,15–17]. Titanium dioxide (TiO_2) as anode materials for LIBs possesses the advantages of low-cost, environmental benignity and easiness to process via sol–gel process [17]. Compared to conventional bulk material, the nanostructured TiO_2 has advantages like the large specific surface area and short diffusion length, and thus leading to a faster charging/discharging rate [18,19]. Among the fabrication approaches, electrospinning is one of the most promising methods to generate nanostructured TiO_2 in large scale with a relatively inexpensive cost and high specific surface area [20–23]. Noteworthy the theoretical capacity of TiO_2 is only ~335 mAh g^{-1}, which is much lower than the theoretic capacity of Si (4200 mAh g^{-1}) [8–10].

Herein, silicon/graphite (Si/C) micro-platelets embedded in TiO_2 nanofibers are fabricated via a facile electrospinning technique. After being thermally annealed in air, part of the graphite embedded in composite nanofibers can be oxidized to generate free space for volume expansion during the lithiation process of silicon. In addition, the titanium oxide shell is beneficial for creating stable SEI films which can further enhance Coulombic efficiency and cycling performance. This type of composite fibers as LIB anode possesses the advantages of high capacity, long cycle life and relatively low fabrication cost compared to other nanostructured silicon materials (nanoparticles, nanowires and nanotubes, as well as porous silicon).

2. Experimental

2.1. Fabrication of Si/C/TiO_2 and TiO_2 nanofibers

First, 1 g Polyvinylpyrrolidone (1.3 M MW, Sigma Aldrich) was dissolved in 10 mL absolute ethanol. Meanwhile, 1 g Titanium (IV) isopropoxide (sigma Aldrich) and 0.1 g, 0.3 g, 0.5 g or 3 g Si/C microplatelets was mixed well with 3 mL glacial acid (HOAc, Sigma Aldrich) and 3 mL absolute ethanol by stirring and keeping under sonication for 10 min. Then these two solutions were mixed together and electrospun into nanofibers using a homebuilt electrospinning setup. The electrospinning working parameters were as follows: applied voltage is direct current (DC) 25 kV (Spellman P/N230-30R); distance between the syringe needle (16 gauge, Air-Tite Products Co.) containing the solution and the grounding collector (aluminum foil) is 12 cm; and pumping rate of syringe was 3 mL h^{-1}. The syringe pump was purchased from New Era Pump Systems Inc. (NE-1000). As-fabricated composite nanofibers were annealed at 540 °C in air for 12 h to remove organic polymers using a Lindberg Blue tube furnace, resulting in the formation of inorganic TiO_2 nanofibers (NFs). The general fabrication scheme for Si/C/TiO_2 composite nanofibers is listed in Fig. 1. The samples prepared using 0.1 g, 0.3 g, 0.5 g and 3 g silicon/graphite micro-platelets are named as SS-1, SS-2, SS-3 and SS-4 in this article, respectively. The fabrication method for TiO_2 nanofibers is similar to that of composite Si/C/TiO_2 NFs except that no Si/C micro-platelets were added.

2.2. Electrode preparation

The preparation of Si/C/TiO_2 and TiO_2 NF electrodes includes slurry making, casting, and drying. Typically, the active materials, Si/C/TiO_2 nanofibers, and carbon black were added into the solution of polyvinylidene difluoride (PVDF) dissolved in *N*-methy-2-pyrrolidone (NMP), with continuously stirring to make solid particles well dispersed in the slurry. The slurry was then coated onto Cu foil (current collector). Next, the electrode was dried at 75 °C for 4 h, followed by being dried at 75 °C in vacuum oven overnight. To completely remove the moisture, the electrodes were dried at 120 °C in the vacuum oven for at least 4 h before the cell assembly. The final solid electrodes are composed of 10 wt.% PVDF, 8 wt.% carbon black, 82 wt.% active materials. The NF electrodes were cut into disks of 1.6 cm^2, and then assembled in 2032-type coin cells using lithium metal as counter electrodes. The electrolyte solution containing 1.2 mol L^{-1} $LiPF_6$ in ethylene carbonate (EC)/ethyl methyl carbonate (EMC) (3/7 by weight) was used in all cells.

2.3. Characterization of Si/C/TiO_2 and TiO_2 nanofibers

As-fabricated nanofibers were characterized using Field Emission Electron Microscopy (JEOL JSM-7600F) attached with OXFORD Energy Dispersive Spectroscopy (EDS) for elemental analysis. The samples were coated with a layer of thin gold film using Denton Desktop sputtering machine for SEM imaging. Samples were also characterized by powder X-ray diffractometer (XRD) using a Bruker D8 Advance diffractometer with Cu Kα radiation (=1.5406 Å) to identify the phase and elemental composition of these nanofibers. To collect information about the elemental composition, these nanofibers were also analyzed by Thermogravimetric Analyzer (TGA) using the thermal analyzer (NETZSCH STA 449 F3).

2.4. Electrochemical characterizations

Galvanostatic cycling tests of the Li/NFs electrode half-cells were conducted using a Maccor series 4000 potentiostat and applying constant currents at room temperature. Initially, 3 formation cycles with an approximated 0.1C current were applied to the cells to

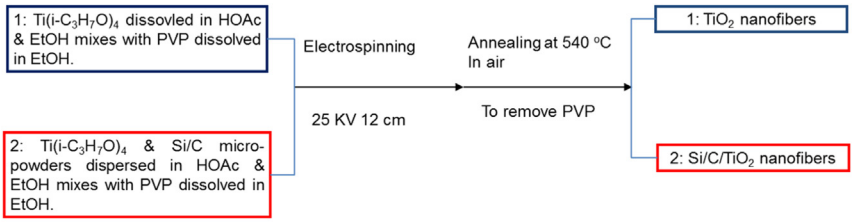

Fig. 1. The general fabrication scheme for pure TiO_2 nanofibers and composite Si/C/TiO_2 nanofibers.

obtain the exact capacity of the cells, and then the exactly calculated 0.1C current was applied to cells for cycle life measurements. The voltage window applied to Li/NFs half cells was 0.01–2 V (vs. Li/Li^+) during formation cycles, while 0.01–1.5 V (vs. Li/Li^+) for cycling tests.

3. Results and discussion

3.1. Fabrication and characterization

TiO_2 NFs were fabricated for control experiments. The diameters of TiO_2 inorganic NFs range from 300 to 800 nm as shown in Fig. 2a. These nanofibers are interwoven into a network structure, possessing a high surface to volume ratio, and thus would benefit a faster charging/discharging rate. Fig. 2b shows the scanning electron microscopy (SEM) images of silicon/graphite micro-platelets, whose thickness is about 300 nm. The mass ratio of silicon to carbon for these micro-platelets is 8:92 as determined from energy dispersive spectroscopy (EDS) measurements (Supporting information 1). Fig. 2c–e are SEM images of Si/C/TiO_2 composite nanofibers which were prepared using 0.1 g, 0.3 g and 0.5 g Si/C micro-platelets, respectively, and annealed at 540 °C in air for 12 h. Noteworthy, these samples annealed at 540 °C in air still contain large content of crystalline graphite as determined by TGA and PXRD analysis, which will be discussed later. Fig. 2f shows the morphology of the composite NFs which were prepared using 3 g Si/C micro-platelets and annealed in air at 540 °C for 24 h, followed by 700 °C anneal in air for 2 h. These micro-platelets are interconnected to each other through TiO_2 nanofibers. It should be pointed out that we increased the anneal temperature and time, with an attempt to further increase the free volume between Si core and TiO_2 shell, thus more efficiently accommodating the nearly 300% volume change during the silicon lithiation process. Powder X-ray diffraction (XRD) was employed to characterize the structure, phase and crystallinity of these NFs. TiO_2 in both pure and composite NFs are of rutile phase as confirmed by powder XRD patterns (JCPDS No.: 21-1276 and Fig. 3). The sharp peak seen around 26° for all samples containing Si/C micro-platelets indicates that the carbon is in the form of highly crystalline graphite (JCPDS No.: 41-1487; graphite (002)). The cubic silicon (111) peak is shown at ~28° for Si/C micro-platelets (JCPDS No.: 27-1402).

By combining EDS and thermogravimetric analysis (TGA) data, we can accurately determine the mass ratio of Si: C: TiO_2 in these composite NFs, and thus the accurate gravimetric capacity of silicon and graphite in these NFs can be attained. From TGA data (Fig. 4), it can be seen that the graphite in these samples don't experience

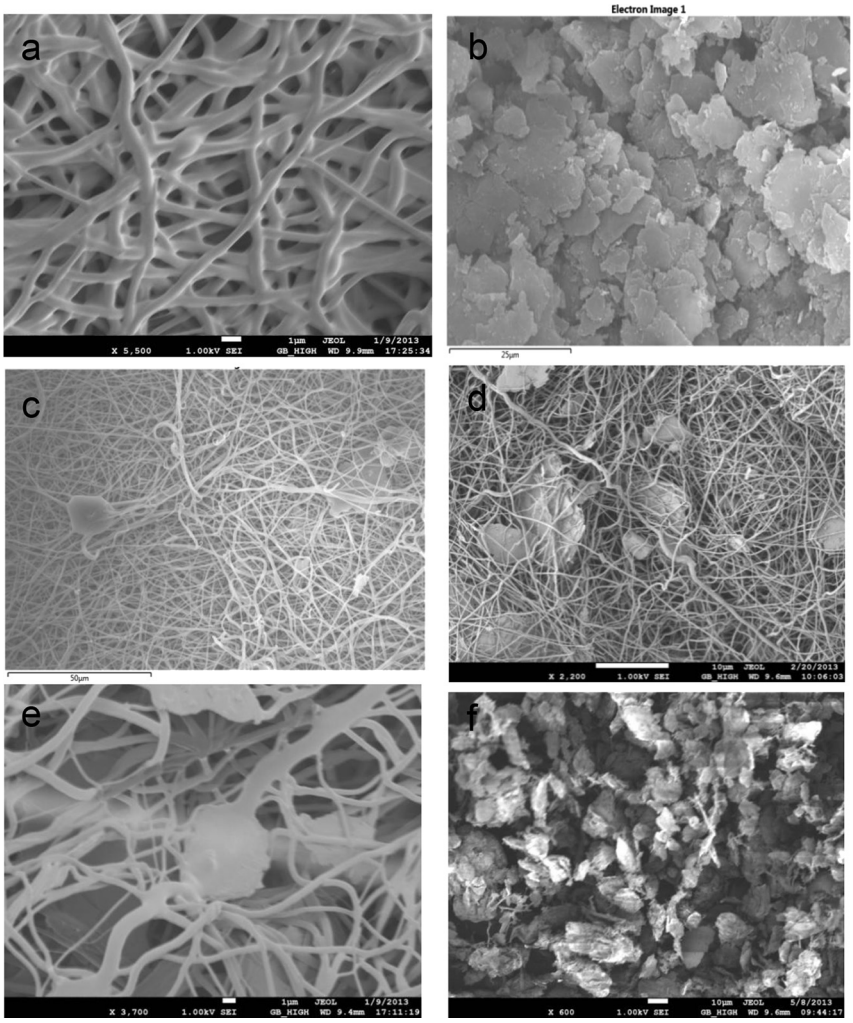

Fig. 2. Scanning electron microscopy images of (a) pure TiO_2 nanofibers; (b) 8 wt.%Si@92 wt.% graphite micro-platelets; (c) nanofibers fabricated using 0.1 g Si/C micro-platelets and annealed in air for 12 h at 540 °C (SS-1); (d) nanofibers fabricated using 0.3 g Si/C micro-platelets and annealed in air for 12 h at 540 °C (SS-2); (e) nanofibers fabricated using 0.5 g Si/C micro-platelets and annealed in air for 12 h at 540 °C (SS-3); (f) nanofibers fabricated using 3 g Si/C micro-platelets and annealed in air for 24 h at 540 °C, followed by 700 °C anneal in air for 2 h (SS-4).

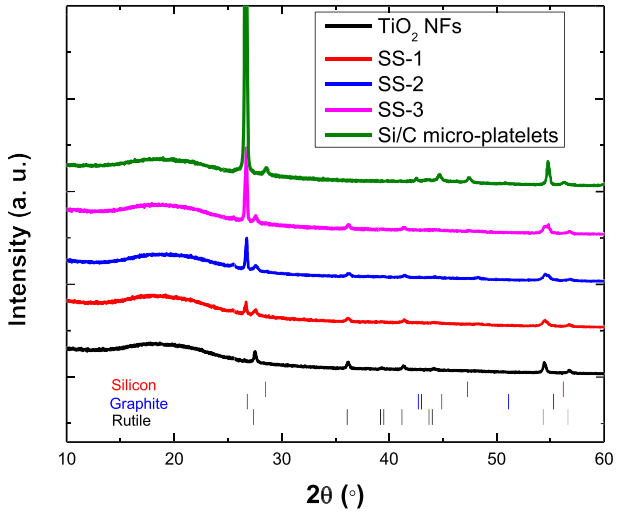

Fig. 3. Powder XRD of Si/C micro-platelets, pure TiO_2 and Si/C/TiO_2 composite NFs. Standard powder XRD patterns of graphite, cubic silicon and rutile TiO_2 are added for direct comparison.

significant oxidation until ~700 °C. Therefore we chose 700 °C to anneal sample SS-4 so that large enough free space can be created to efficiently accommodate the huge volume expansion during the silicon lithiation process. Noticeable, the graphite concentration in SS-4 is relatively high, but the graphite to silicon mass ratio is lower than other samples (Table 1), indicating that more graphite has been oxidized at an elevated temperature (700 °C) as compared to 540 °C. The reason to use such a large amount of Si/C micro-platelets (3 g for SS-4) is to increase the specific capacity of the electrode since rutile TiO_2 has a much lower theoretical capacity than silicon and graphite.

Table 1
Summary of electrochemical performance of Si/C/TiO_2 composite NF electrodes.

Sample	C (wt %)	Si (wt %)	TiO_2 (wt%)	Specific capacity of Si/C[a] (mAh g^{-1})	Specific capacity of Si[b] (mAh g^{-1})	ICL (%)[c]
TiO_2 NFs	0	0	100	0	0	73.6
SS-1	18.84	2.35	78.81	579	2416	61.6
SS-2	29.37	4.89	65.74	420	841	59.3
SS-3	46.27	6.23	47.50	439	1098	46.8
SS-4	63.29	13.71	23.00	610	1805	27.4

Note: SS-1, SS-2, SS-3 and SS-4 are defined in the experimental part. The specific capacity of all NF electrodes is calculated using the third charge process data.

[a] Specific capacity is equal to the capacity divided by the mass of silicon and graphite (the capacity contribution from TiO_2 is excluded and its specific capacity is 83.3 mAh g^{-1}).

[b] Specific capacity is equal to the capacity divided by the mass of silicon (the capacity contribution from TiO_2 and graphite are excluded and their specific capacities are 83.3 mAh g^{-1} and 350 mAh g^{-1}, respectively).

[c] Irreversible capacity loss (ICL) is derived from the first formation cycle including the contribution from TiO_2 nanofibers.

3.2. Electrochemical performance of NFs as LIB anodes

TiO_2 is utilized as a protection material to stabilize the electrochemical performance of silicon in these composite NFs. It is critical to accurately determine the capacity and mass percentage of TiO_2 in

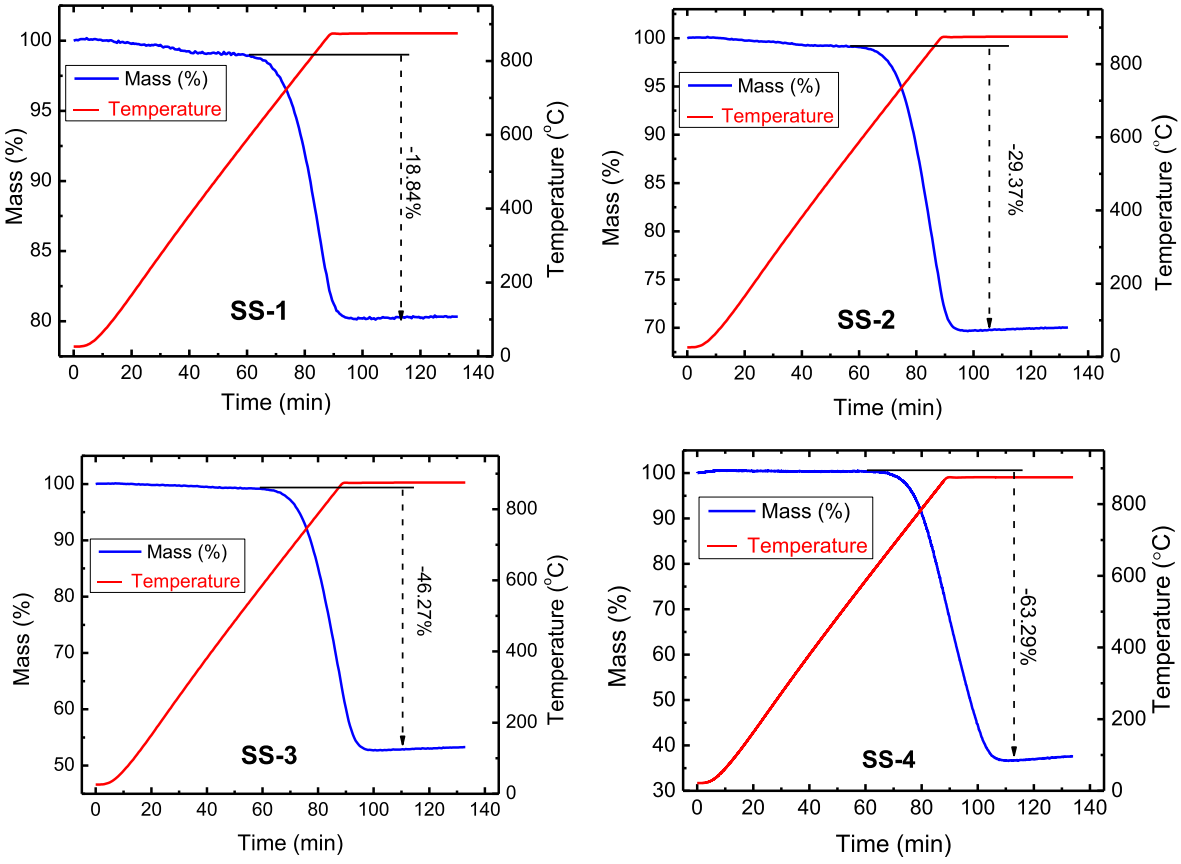

Fig. 4. TGA spectra combined with EDS analysis to accurately obtain the mass ratios of Si:C:TiO_2 for various types of nanofibers.

these composite NFs. So the specific capacity contributed from Si and graphite can be precisely calculated. Pure TiO_2 NFs were fabricated into LIB anode to determine their specific capacity. Their electrochemical performance was tested under the same conditions as those applied to Si/C/TiO_2 composite NF anodes (SS-1, SS-2, SS-3 and SS-4). As mentioned above, TiO_2 is a very stable anode material for lithium ion batteries with an operating voltage window of 1–2 V. Although it is difficult for Li ions to insert into micrometer-sized rutile phase TiO_2 due to kinetic restrictions, nanostructuring TiO_2 can strongly increase both the capacity ($Li_{0.85}TiO_2$ at 25 °C, 335 mAh g^{-1}) and the rate capability. [24] From the voltage profiles (Fig. 5a), a long plateau at ~1.25 V followed by a long and gradually decreasing slope can be clearly seen during the first discharge process. However, this plateau and long slope are replaced by short slopes during the following charge and discharge process, indicating there is an irreversible phase transformation of the material [25]. More details about the electrochemical behaviors of TiO_2 nanofibers electrode can be obtained by analyzing the differential capacity vs. voltage plot (Fig. 5b). One sharp (~1.17 V) and 3 weak (~1.73 V, 1.39 V, and 0.79 V) peaks can be observed during the first discharge process, but there are no peaks during the following cycles regardless of either charge or discharge process. Peaks at 1.39 and 1.17 V can be ascribed to the irreversible phase transformation from TiO_2 to $LiTiO_2$ [25–27]. The peak observed below 1 V (0.79 V) is assigned to the irreversible reduction of the electrolyte [28]. Peak shown at 1.73 V is consistent with reversible lithium insertion to form Li_xTiO_2. [28] In addition, the specific capacity is about 350 mAh g^{-1} during the first discharge process, most of which is derived from the SEI formation. This capacity is dramatically reduced to ~83 mAh g^{-1} during the following cycles, which is corresponding to an insertion of 0.21 mol Li ions into one mole TiO_2. The capacity of TiO_2 NF anode maintains stable after the first formation cycle, thus benefiting an accurate determination of capacity contribution from TiO_2 in those composite nanofibers. Our specific capacity is very close to the value reported by literature [27,29]. Noteworthy the capacity of TiO_2 NFs is very stable with less than 5% decrease after 50 cycles as reported by literature [29]. In Ref. [29], the PVP to titanium (IV) isopropoxide mass ratio is 1:3.3 as compared to 1:1 in this paper. The ethanol to acetic acid volume ratio is 7:1 in ref. 29 while our ratio is 4.3:1. The pumping rate of syringe is 2 mL h^{-1} in Ref. [29] and ours is 3 mL h^{-1}.

Fig. 6 shows the electrochemical behaviors of Si/C/TiO_2 composite NF electrodes. For all NF samples, there is a plateau at ~1.25 V followed by a slope on the first discharge process. Similar to the pure TiO_2 NF electrode, the plateau is replaced by a slope after the first cycle. Additionally, a long plateau is found below 0.2 V. The length ratio of the plateau at 1.25 V to the plateau below 0.2 V decreases with increasing the amount of Si/C micro-platelets in these composite NF electrodes (Fig. 6a, c, e and g). From the differential capacity vs. voltage plots, peaks located at ~1.73 V, 1.39 V, 1.17 V and 0.79 V can be clearly seen for the first discharge process, which are characteristics of lithium insertion into TiO_2. Similar to pure TiO_2 NF electrode, these peaks disappeared during the following cycles. With the reduction of the mass percentage of TiO_2 in these composite NFs, the intensity of these peaks is decreasing gradually (Fig. 6f and h). Besides these characteristics peaks associated with insertion of lithium ions into TiO_2 nanofibers, three peaks located at ~0.17 V, 0.06 V and 0.03 V are also observed during the first discharge process for all Si/C/TiO_2 composite NF electrodes, and these peaks are present for all the following cycles (Fig. 6b, d, f and h). The long plateau below 0.2 V in the voltage profiles and peaks below 0.2 V in the differential capacity plots are associated with the insertion of lithium ions into carbon and silicon components for these composite NF samples. When the mass percentage of TiO_2 in these composite NFs is ~79%, the reversible capacity is only ~200 mAh g^{-1}. Herein, the reversible capacity is equal to the total capacity divided by total mass of composite NFs (*silicon, carbon and TiO_2*). The reversible capacity of these composite NF electrodes increases gradually while the mass percentage of TiO_2 in these composite nanofibers is decreasing. The gravimetric capacity can reach ~420 mAh g^{-1} when the mass percentage of TiO_2 nanofibers is reduced to ~25%. Reducing the mass percentage of TiO_2 in these nanofibers can also reduce the irreversible capacity loss (ICL) for the first cycle (Table 1). It is well known that nanostructured TiO_2 can cause severe first discharge ICL due to reactive TiOH and TiO surface sites that can cause unwanted electrolyte degradation and irreversible trapping of lithium ions. [17] If neglecting the capacity contribution from TiO_2, the specific capacity of Si and graphite in these composite NF electrodes increases from 420 to 610 mAh g^{-1} while the mass percentage of TiO_2 in these nanofibers is reduced from ~66 to ~23 wt.% (Table 1). All these data are pointing to one conclusion that increasing the content of Si and carbon could effectively increase the specific capacity of composite NF electrodes.

The higher mass ratio of Si to C in these composite NFs can help improve the durability of the derived electrodes. As shown in Fig. 7, the capacity retention after 55 cycles is only about 65% when the Si to C mass ratio is 0.125 (SS-1). The capacity retention increases gradually to ~71% and 74%, respectively while the mass ratios of Si to C are further increased to 0.166 and 0.135 (SS-2 and SS-3). For the SS-4 sample with a Si to C mass ratio of 0.217, the specific capacity after 55 cycles is as high as ~677 mAh g^{-1}, which is ~94% of the initial value. Compared to SS-2 sample, the relative concentration of Si/C in SS-3 sample is much higher. It is highly possible that silicon/graphite micro-platelets will agglomerate more seriously in SS-3, which can affect the permeation of oxygen and thereby

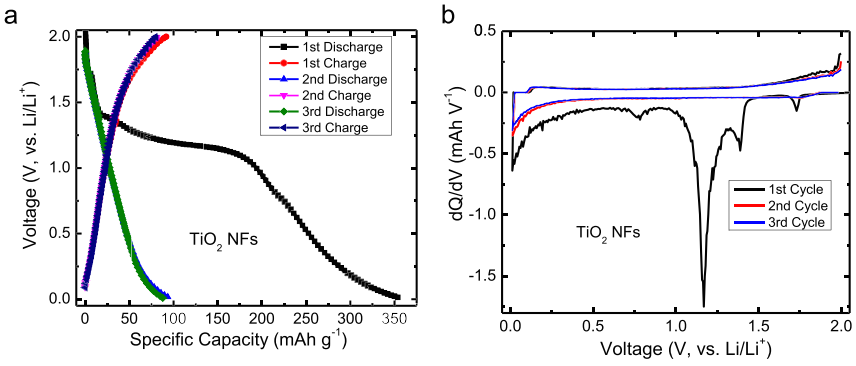

Fig. 5. Electrochemical performance of TiO_2 nanofiber anode. (a) Voltage vs. capacity; and (b) differential capacity vs. voltage.

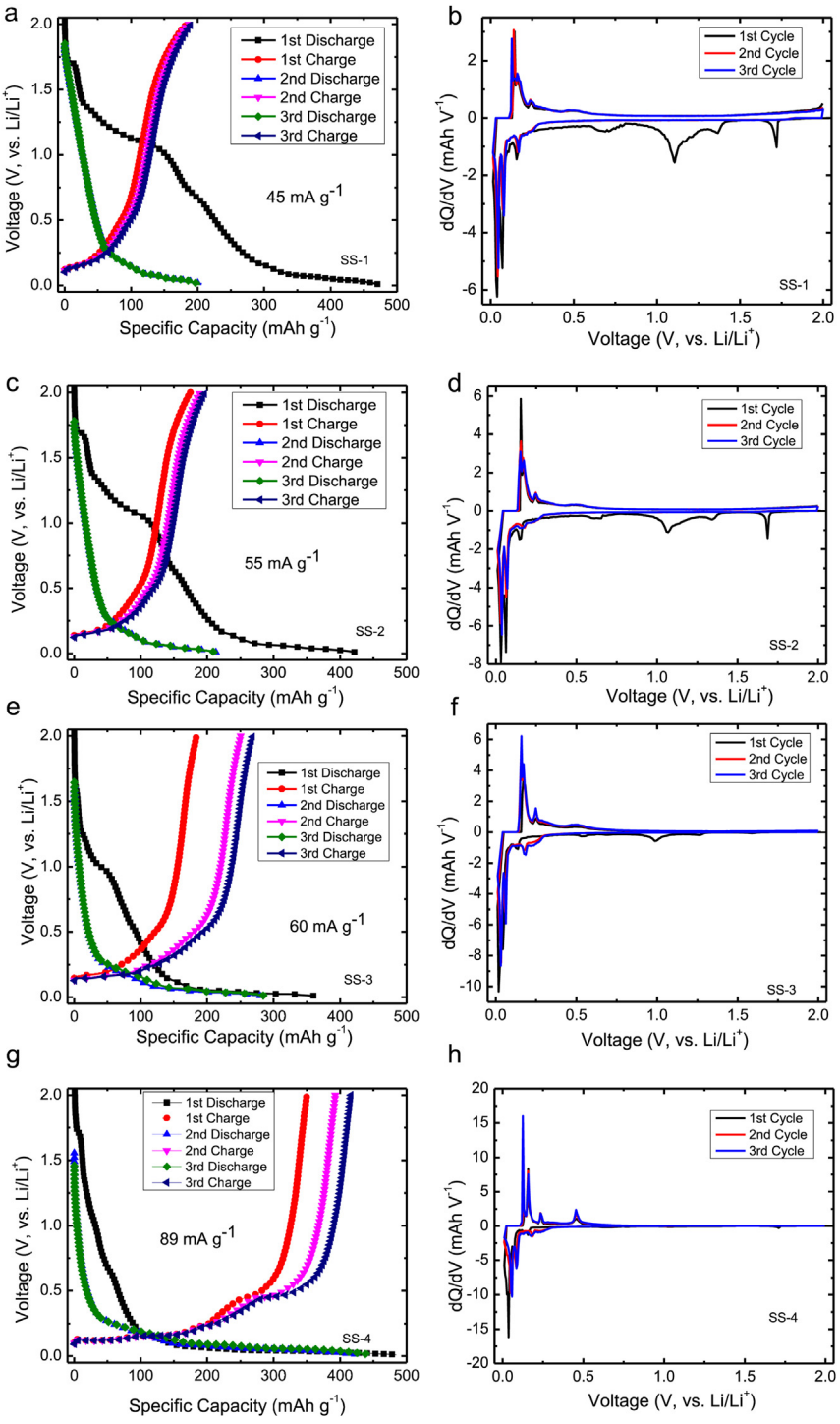

Fig. 6. Electrochemical performance of Si/C/TiO_2 composite NFs electrodes with various contents of silicon and carbon (SS-1, SS-2, SS-3 and SS-4). The specific capacity is calculated here as the total capacity divided by the mass of titania, silicon and graphite.

reduce the oxidation rate of graphite. That is the reason why the Si/C ratio for SS-2 is larger than SS-3. As for SS-1, the concentration of TiO_2 is so high that it can function like a thick protection lay to slow down the oxidation of graphite, resulting in a low Si to C ratio. In the case of SS-4, it was annealed at much higher temperature (700 °C vs. 540 °C), leading to a more efficient oxidation of graphite and high Si/C ratio.

Compared with the formation cycles, the specific capacity of most samples increase except for SS-1 even as the higher cut-off voltage was decreased from 2 V to 1.5 V. It is because that the current density used in the cycling test is lower than the one used in the formation cycles. The current density used in formation cycles is estimated using the theoretical specific capacity of Si, C and TiO_2, whereas the current density used in the cycling test is calculated from the specific capacity of the third formation cycle. It should be noted that a higher Si to C ratio is corresponding to a larger free space in the composite NFs because more graphite is removed by oxidation, thus more efficiently accommodating the

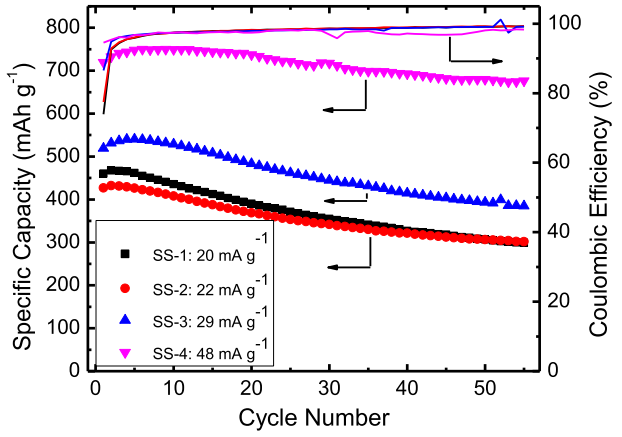

Fig. 7. Cycling performance of Si/C/TiO_2 composite NF electrodes with different mass percentage of silicon and graphite. Specific capacity for all NF electrodes is equal to the capacity contributed from Si and C divided by the total mass of Si and C. Note: the charging/discharging current is lower than the one used for the three formation cycles.

volume change. We also opened the cycled cells in argon glove box to retrieve Si/C/TiO_2 composite NF electrodes. No cracks were observed for these cycled NF electrodes under SEM examinations, and active materials covered with SEI films can be clearly seen as compared with electrodes without cycling (Supporting information 2). This fact indicates that these composite NF electrodes possess excellent mechanical properties to tolerate the stress generated during silicon lithiation and delithiation process. Our control experiment shows that the cycling performance of Si/graphite micro-platelet anode is quite poor, whose specific capacity decreased by 71.9% to 116 mAh g^{-1} in 30 cycles at a current density of 83 mA g^{-1} (Supporting information 3). Finally, the relatively high specific capacity for SS-1 sample (compared to SS-2 sample) might be derived from the unique networking nanofiber structure, which can prevent some fractured Si micro-platelets from leaching out into electrolyte solution, eventually resulting in the capacity loss. Increase the content of Si (SS-2 sample); however, some fractured Si can still leach out because it is over the protection capacity of this networking nanofiber structure. Additionally, the relatively high Si/graphite micro-platelet concentration in SS-2 sample can cause more serious agglomeration of these micro-platelets, thus leading to an insufficient charging and a lower capacity as compared to SS-1 sample.

4. Conclusion

A facile electrospinning method has been developed to fabricate Si/C/TiO_2 composite nanofibers with variable Si to TiO_2 ratios for lithium ion battery application. Pure rutile TiO_2 nanofibers can only provide an 83 mAh g^{-1} specific capacity; whereas Si/C/TiO_2 composite nanofibers possess a specific capacity of ~720 mAh g^{-1}. More than 94% capacity can be maintained after 55 cycles, indicating that structurally stable TiO_2 coating does protect Si from leaching into electrolytes and provide relatively stable SEI films. The free space between Si core and TiO_2 shell can be well controlled by varying the annealing time and temperature, thus providing a unique approach to generate three-dimensional structures which can efficiently accommodate the huge volume expansion during silicon lithiation process and improve the cycle life of micro-scale silicon material for LIB applications. This important finding can provide a beneficial guidance for future lithium ion battery anode design which doesn't require the usage of relatively expensive nanostructured silicon materials.

Acknowledgments

JW and TT sincerely acknowledge the generous Start-up Funding provided by Georgia Southern University. QL and WQL greatly appreciate the financial support from David Howell and Peter Faguy of the U.S. Department of Energy's Office of Vehicle Technologies Program. Part of SEM imaging was accomplished at the Electron Microscopy Center for Materials Research at Argonne National Laboratory, a U. S. Department of Energy Office of Science Laboratory operated under Contract No. DE-AC02-06CH11357 by UChicago Argonne, LLC.

Appendix A. Supplementary data

Supplementary data related to this article can be found at http://dx.doi.org/10.1016/j.jpowsour.2014.02.047.

References

[1] C.-M. Park, J.-H. Kim, H. Kim, H.-J. Sohn, Chem. Soc. Rev. 39 (2010) 3115–3141.
[2] J.B. Goodenough, Acc. Chem. Res. 46 (2013) 1053–1061.
[3] A. Midilli, I. Dincer, M. Ay, Energy Policy 34 (2006) 3623–3633.
[4] K. Caldeira, A.K. Jain, M.I. Hoffert, Science 299 (2003) 2052–2054.
[5] M. Armand, J.M. Tarascon, Nature 451 (2008) 652–657.
[6] C. Daniel, JOM J. Miner. Metal. Soc. 60 (2008) 43–48.
[7] J. Li, C. Daniel, D. Wood, J. Power Sources 196 (2011) 2452–2460.
[8] Z. Yang, D. Choi, S. Kerisit, K.M. Rosso, D. Wang, J. Zhang, G. Graff, J. Liu, J. Power Sources 192 (2009) 588–598.
[9] X. Su, Q. Wu, X. Zhan, J. Wu, S. Wei, Z. Guo, J. Mater. Sci. 47 (2012) 2519–2534.
[10] C.K. Chan, H.L. Peng, G. Liu, K. McIlwrath, X.F. Zhang, R.A. Huggins, Y. Cui, Nat. Nanotechnol. 3 (2008) 31–35.
[11] H. Wu, Y. Cui, Nano Today 7 (2012) 414–429.
[12] J.B. Bates, N.J. Dudney, B. Neudecker, A. Ueda, C.D. Evans, Solid State Ionics 135 (2000) 33–45.
[13] J.K. Lee, K.B. Smith, C.M. Hayner, H.H. Kung, Chem. Commun. 46 (2010) 2025–2027.
[14] R. Yi, F. Dai, M.L. Gordin, H. Sohn, D. Wang, Adv. Energy Mater. 3 (2013) 1507–1515.
[15] R. Yi, F. Dai, M.L. Gordin, S. Chen, D. Wang, Adv. Energy Mater. 3 (2013) 295–300.
[16] X. Su, Q. Wu, J. Li, X. Xiao, A. Lott, W. Lu, B.W. Sheldon, J. Wu, Adv. Energy Mater. 4 (2014) 1300882.
[17] A.G. Dylla, G. Henkelman, K.J. Stevenson, Acc. Chem. Res. 46 (2013) 1104–1112.
[18] Z. Yang, J. Zhang, M.C.W. Kintner-Meyer, X. Lu, D. Choi, J.P. Lemmon, J. Liu, Chem. Rev. 111 (2011) 3577–3613.
[19] A. Primo, A. Corma, H. Garcia, Phys. Chem. Chem. Phys. 13 (2011) 886–910.
[20] D. Li, Y. Xia, Nano Lett. 3 (2003) 555–560.
[21] J. Wu, J.L. Coffer, Chem. Mater. 19 (2007) 6266–6276.
[22] J. Wu, J.L. Coffer, J. Phys. Chem. C 111 (2007) 16088–16091.
[23] J. Wu, J.L. Coffer, Y. Wang, R. Schulze, J. Phys. Chem. C 113 (2008) 12–16.
[24] Y.S. Hu, L. Kienle, Y.G. Guo, J. Maier, Adv. Mater. 18 (2006) 1421–1426.
[25] M. Pfanzelt, P. Kubiak, M. Fleischhammer, M. Wohlfahrt-Mehrens, J. Power Sources 196 (2011) 6815–6821.
[26] M.A. Reddy, M.S. Kishore, V. Pralong, V. Caignaert, U.V. Varadaraju, B. Raveau, Electrochem. Commun. 8 (2006) 1299–1303.
[27] S.W. Kim, T. Kim, Y.S. Kim, H.S. Choi, H.J. Lim, S.J. Yang, C.R. Park, Carbon 50 (2012) 3–33.
[28] M. Marinaro, M. Pfanzelt, P. Kubiak, R. Marassi, M. Wohlfahrt-Mehrens, J. Power Sources 196 (2011) 9825–9829.
[29] M.V. Reddy, R. Jose, T.H. Teng, B.V.R. Chowdari, S. Ramakrishna, Electrochim. Acta 55 (2010) 3109–3117.